REPORT OF GROUP IV

INTERACTION REGIONS AND DETECTORS FOR ELECTRON PROTON EXPERIMENTS AT 140 GeV + 20 TeV

Convenor : G. Weber

S. Conetti, Fang-Shou-Hsien, K. Hübner, P.G. Innocenti, Y. Kimura, I.A. Savin, R. Turlay, W.A. Wenzel, E.J.N. Wilson and Y. Yamaguchi.

1. INTRODUCTION

Electron proton scattering experiments have proven a powerful means for exploring the structure of hadrons, and have given the first direct experimental proof of pointlike behaviour of quarks in the nucleon. The great impact these pioneering experiments have had on development of particle research has created an ever growing interest in doing lepton nucleon experiments at the highest possible C.M. energies. Since with fixed target experiments the C.M. energy increases only with the square root of the beam energy, e-p colliding beam devices become increasingly attractive for C.M. energies beyond $\sim$ 100 GeV.

Therefore, assuming a 20 TeV proton storage ring[1] will be constructed in the future, it is very tempting to investigate the possibility of colliding it with a high energy electron beam. It was the task of the present study to investigate machines, interaction regions and detector devices for ep colliding beam experiments at 140 GeV + 20 TeV. The results are very encouraging in that they show that with the present day technology an ep storage ring for 140 GeV + 20 TeV can be constructed with a luminosity sufficient to study the electron nucleon interaction at momentum transfers $\sim 10^6$ GeV^2. As explained in chapter 2 below, this corresponds to probing the nucleon at distances smaller than 10^{-17} cm, roughly a factor 100 below the present limits and about an order of magnitude below that of the proposed HERA[2] machine.

In chapter 3.1 the main parameters of a circular ep machine are presented. The machine consists of the proton ring of the 20 TeV pp-collider[1] and a 140 GeV electron ring housed in the same tunnel. A design example is worked out based on rather conservative values for the beam-beam tune-shifts and on a small crossing angle. A luminosity of 10^{31} cm^{-2}sec^{-1} is obtained. The lay-out of the interaction region, the most crucial point in the design of an ep machine, is presented in some detail. Since the electron ring and the proton ring do not have common elements, the e-ring can be filled with positrons or electrons requiring only a minimum change-over time. Polari-

sation of the $e^{\pm}$ beam is discussed. Electron-proton collisions by means of an electron linac and the proton ring are considered in section 3.2. A preliminary set of parameters is presented. The main shortcoming of this solution is that only one, maybe two, interaction regions are available and the required RF power is excessive. The linac is based on parameters similar to those of the $e^{\pm}$linear colliders discussed elsewhere in this proceedings[3].

In chapter 4 the kinematics for ep collisions is discussed. Using standard expressions[4] for the structure functions of the nucleon the counting rates obtainable with the collider are compared with those of a fixed target muon experiment discussed in these Proceedings[5].

A general purpose detector based on electromagnetic and hadronic shower calorimetries is presented in chapter 5, where also a method of detecting particles from the target fragmentation[6] is presented. In chapter 6 the problem of radiative corrections is discussed and the need for calculating the higher order corrections is pointed out.

2. ELECTRON PROTON PHYSICS AT 140 GeV + 20 TeV

Fig. 1 shows a plot of Q^2 versus ν for some existing and proposed fixed target ep and μp facilities, as well as for colliding beam projects. The ν- and Q^2 values obtainable with colliders are seen to exceed those of fixed target experiments by several orders of magnitude. F.e. the 30 GeV + 820 GeV ep machine HERA extends the ν- and Q^2-values obtainable at the SPS by more than a factor 100, and the 140 GeV + 20 TeV collider brings another increase by two orders of magnitude. A 15 TeV muon beam impinging on a stationary target[5] is roughly equivalent to the 23 GeV + 300 GeV ep collider TRISTAN[7]. It is obvious from Fig. 1 that the ep machine discussed here will open a realm of particle physics inaccessible by any other means.

The physics with ep storage rings at C.M. energies of a few hundred GeV has been described in an article by C. Llewellyn-Smith and B. Wiik[8] and in a number of ECFA studies[9]. Some of the physics that might be done with the 140 GeV + 20 TeV ep collider has been discussed in a contribution to this workshop by Kimura et al.[10]. The most recent study was on the ep storage ring HERA proposed[2] for DESY, which, if authorized in 1981, will become operational in 1987/88. It will probably take a decade longer before the 140 GeV + 20 TeV collider becomes operational. Very likely the present knowledge of particles and their interactions will undergo considerable changes till that time and therefore discussions of the physics to be done with the ICFA collider have to be kept rather general.

Let us recall that present lepton nucleon scattering experiments using incident beams of high energy electrons, muons and neutrinos on stationary

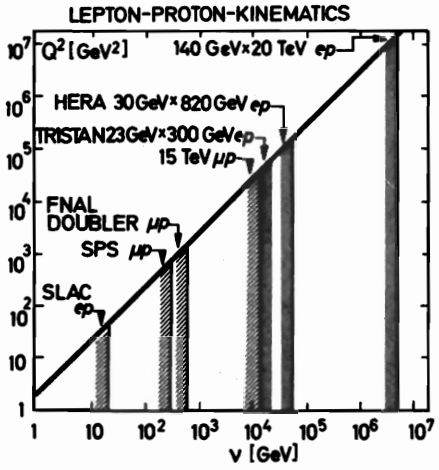

Fig. 1 Q^2 versus ν plot for fixed target lepton nucleon scattering facilities and for ep storage rings.

targets are probing the nucleon down to distances of a few times 10^{-16}cm. HERA[2] will permit the nucleon to be probed down to distances roughly a factor 10 smaller than the present experiments and somewhat further than the fixed target 15 TeV muon experiment[5] considered by group VI. The 140 GeV + 20 TeV ep collider will extend our knowledge of the nucleon structure down to distances below 10^{-17} cm, about a factor 100 below the present limit. In studying the short distance behavour of the lepton - nucleon interaction one is bound to encounter new phenomena associated with large mass particles, perhaps some of the many objects postulated by current theories : Excited quarks and leptons, quarks and leptons with exotic spin and charge, free quarks and free gluons, colour sextetts, technicolour, Higgs scalars, quark and lepton constituents, monopoles, right handed W- and Z-bosons, etc. In order to measure right handed and left handed currents separately the availability of electron and positrons in both helicity states is highly desirable.

3. ELECTRON PROTON MACHINES

3.1 Circular ep machines

3.1.1 Main parameters

The pp collider group has proposed three magnetic structures. Our example is based on the very strong focussing version of the proton ring because an electron ring of similar parameters, though somewhat less focus-

sing, would provide the required electron emittance. This weaker focussing has also the beneficial effect of making the machine less sensitive. Table I gives the basic machine parameters.

TABLE 1

Main Parameters ep Machine

			p - ring		e - ring
Energy		TeV	20		0,14
Luminosity		$cm^{-2}sec^{-1}$		10^{31}	
Radius		km		12	
Bending radius		km		6,7	
Q			≈240		≈200
Beta functions	β_x^*/β_y^*	m	25/6,3		2,1/0,50
Dispersion functions	D_x^*/D_y^*	m	0		0
Free space for detector		m		±20	
Crossing angle	$2\emptyset$	mrad		3	
Beam size at crossing	σ_x^*/σ_y^*	μm		120/30	
Emittance	ε_x/π	radm	48.10^{-6} *)		$6,9.10^{-9}$
Emittance	ε_y/π	radm	12.10^{-6} *)		$1,9\text{-}10^{-9}$
Bunch-length	σ_s	cm	3		≤3
Beam-beam tune-shift	$\Delta Q_x=\Delta Q_y$		0,0005		0.012
Number of bunches				800	
Total number of particles			5.10^{13}		2.10^{13}
Particles per bunch			$6,3.10^{10}$		$2,5.10^{10}$

*) Normalized emittance $\varepsilon/\pi = \beta_p\gamma_p(2\sigma)^2/\beta$

The beta values at the interaction point and the beam emittance are the same as chosen in the 1978 ICFA workshop[11]. Ample space is provided for the detector. The small crossing angle is necessary to separate the electron and proton beam without common elements. The beam size in the intersection point is very small requiring precise steering of the two beams. The vertical emittance of the proton beam is relatively small but within the range measured at 25 GeV in the CERN PS. The proton bunch-length is obtained by scaling from the SPS. It is sufficiently long to fulfill the longitudinal stability criteria[12]. For the electron bunch-length, an upper limit is given corresponding to a very low synchrotron tune of 0,01. Since doubts have been expressed as to whether the choice of the standard tune-shifts ΔQ_e = 0,06 and ΔQ_p = 0,005 is not too optimistic, a design example using ΔQ_e = 0,012 and ΔQ_p = 0,0005 is presented. This electron tune-shift has been reached experi-

mentally in all $e^{\pm}$ machines in both planes simultaneously; proton tune-shifts in excess of 0,0005 have been reached in bunched beam operation in the ISR[13] with no sign of beam-beam effects. Although the maximum admissible tune-shift in an ep machine is not known for lack of experiments, it is believed that our values are a reasonably safe guess making provisions for the adverse influence of the finite crossing angle and not perfect beam alignment. In order to compensate the drop in luminosity due to the lower tune-shifts, the number of bunches is increased substantially compared with the solution discussed at the 1978 ICFA workshop[11]. Such a high number of bunches is acceptable in a machine where no unwanted crossings can occur since the two beams circulate in two separate rings. The total number of protons is comparable with the number obtained in the CERN SPS and in the main ring of FNAL. The number of particles is lower in the electron ring in order to avoid excessive synchrotron radiation loss. Since the number of protons per bunch is half the number obtained in the SPS in a stored single bunch, and since the number of electrons per bunch is about 6 times smaller than assumed for LEP, it is believed that the single bunches are stable. Another limit on the number of particles is brought about by multibunch instabilities if the number of bunches is large. The driving term of these instabilities is proportional to the ratio $(N/k_b)/T_b$ where T_b is the time between two bunch passages. It can be seen from Fig. 2 that the ratio pertaining to our example is in the same range as that of the machines in operation or planned.

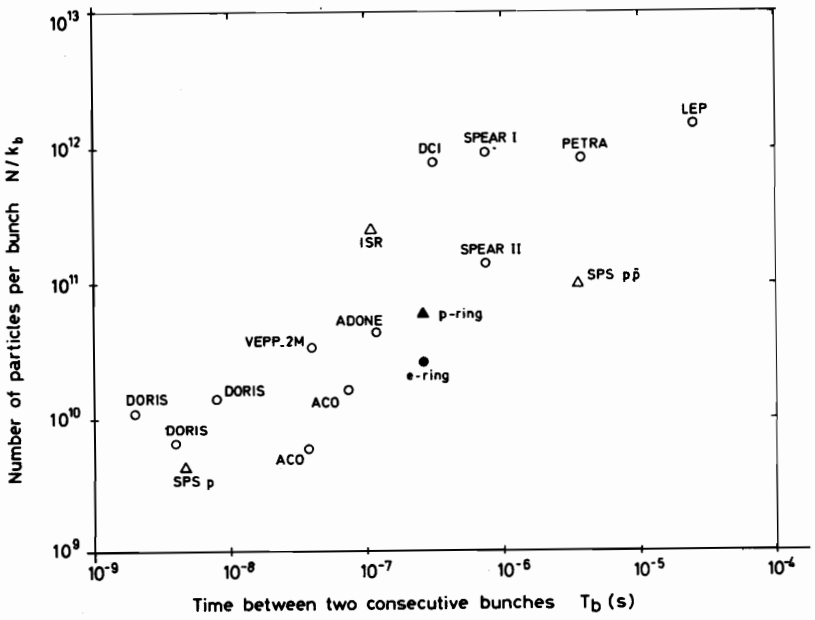

Fig. 2 Comparison with other machines with regard to multi-bunch instabilities

In the electron ring, the synchrotron radiation loss is 5 GeV per turn requiring a superconducting RF structure of about 1 km effective length. The synchrotron radiation power is ∿ 70 MW; the dissipation in the vacuum chamber is 1,7 kW/m which is perfectly acceptable.

3.1.2 Lay-out of the Interaction Region

In order to minimize the loss in luminosity due to the non-zero crossing angle, the beams cross in the horizontal plane. A plan view of the interaction region is shown in Fig. 3.

The beta-functions in the interaction point and the requirement $\beta \leq 1000$ m in the quadrupoles determine the position of the proton doublet. The gradient is 74 T/m in these quadrupoles; the field strength at the inner coil edge is around 3T. The bore of the quadrupoles provides $\pm 6\sigma$ during injection at 400 GeV. It is reasonable to assume that the low beta insertion will be detuned to a higher β^* before injection resulting in a considerably increased aperture margin in the quadrupoles during injection, as the proton beam in the electron doublet will limit the possible tuning range.

Since the beta functions β^* are much lower in the electron ring, the electron doublet, having a modest gradient of ∿ 8,4 T/m, must be close to the interaction point. Its aperture is determined by the proton beam passing through off-axis. The crossing angle is determined in such a way that the electron beam can just clear the proton doublet through a hole in the warm iron yoke of the proton quadrupole[14]. The electron beam is then deviated by a weak bending magnet whose field strength (100 G) is determined by the permissible critical energy (∿100 keV) of the synchrotron radiation falling

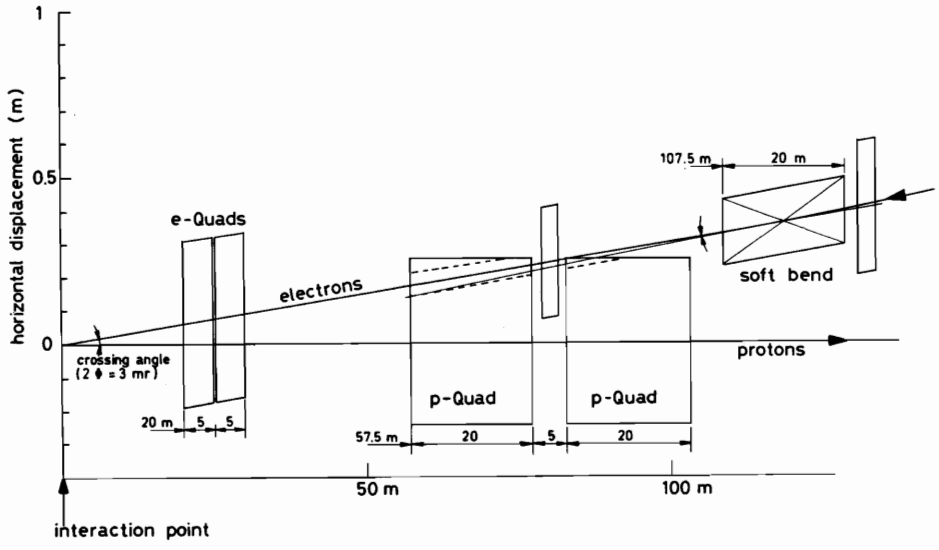

Fig. 3 Plan-view of the interaction region.

into the detector. Since this radiation would give rise to strong background either via (γ,p) events or via backscattering on the walls, it must be reduced by masks placed strategically in the detector. The length of the weak bend is sufficient to prevent the synchrotron radiation, generated in the upstream magnets from passing through the hole (60 mm Ø) in the yoke of the proton quadrupole acting as a radiation shield.

It is not claimed that this lay-out is a unique solution. It is rather a first and certainly incomplete attempt at such energies. It demonstrates the main difficulties the designer is confronted with by this most intriguing part of an ep machine. At this context a scheme for an ep intersection recently proposed by Steffen and Dasskowski[15] for a 30 GeV + 900 GeV collider is worth mentioning. It uses interlaced focussing of the electron and proton beams in which the particles collide head on. Whether this scheme is applicable at the energies considered needs further study.

3.1.3 Beam Polarization

Beam polarization is important for all types of ep experiments except for the measurement of the structure functions. Unfortunately, polarization is not a very transparent topic and, therefore, only some rough estimates could be made.

The polarization time τ_p due to the classical Sokolov-Ternov effect is 16 min at 140 GeV. Since $\tau_p \sim \gamma_e^{-5}$, this mechanism becomes useless at low energy though wigglers[16] or kink-magnets[17] can extend its useful range. If the orbit is not in a plane,the spin precession axis becomes energy dependent. The polarization time by synchrotron radiation is reduced but so also is the equilibrium polarization[18]. This effect, being due to the non-uniform magnetic guiding field, is not included in the 16 min quoted above. Its calculation requires an exact knowledge of the magnetic structure. Apart from synchrotron radiation, the beam can be polarized also by interacting with a circularly polarized photon beam because of the spin dependence of Compton scattering. Although suitable lasers do not yet exist, this is a very promising technique for providing reasonable polarization rates also at low energy where the radiative polarization is too weak.

The equilibrium polarization is determined by the balance between polarization and depolarization. The main depolarization effect is brought about by integer spin resonances. They occur whenever $a\gamma_e = k$ where $a = (g-2)/2 = 1{,}16.10^{-3}$ and k any integer, i.e. with a spacing of 440 MeV in energy. A simple estimate[19] shows that the resonances do not overlap if the peak closed orbit amplitude is less than 10 mm in our case. At lower energy, the energy spread is small and the particle distribution in energy fits between these resonances. However, from about 70 GeV onwards the beam starts to straddle these resonances, the particles will continuously cross

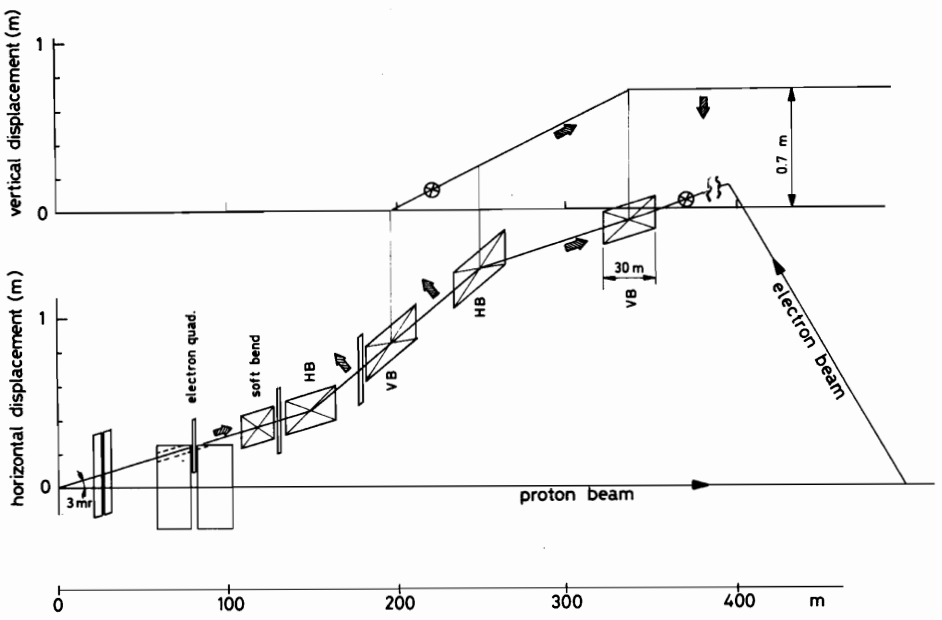

Fig. 4 Elevation and plan view of the interaction region including the magnets used for spin rotation. Bending angle ≈ 5 mrad per magnet.

resonance lines and depolarization will occur. The situation is most adverse at 140 GeV where the energy spread has reached 210 MeV which is comparable to the spacing of the resonances. The more conservative estimates[19] predict that the orbits cannot be controlled accurately enough to make the resonance crossing harmless. For example, the peak closed orbit amplitude should be less than 10 μm at 140 GeV. To overcome this limitation a double Siberian snake must be installed. It makes the spin precession frequency independent of energy and, therefore, does away with the integer spin resonances. However before one definitely resorts to a Siberian snake, which is fraught with other disadvantages, one must scrutinize all other possibilities carefully including more recent work[20] on resonance crossing which seems to be more optimistic.

Radiative polarization provides transversely polarized particles; experiments need longitudinal polarization in the interaction region. Thus ways must be found to rotate the spin by a sequence of magnetic elements into the longitudinal direction[21]. Fig. 4 shows an example. In order to prevent depolarization in these spin-rotating magnets, where spin and magnetic field are not parallel, the magnetic field must be rather low.

The general conclusion is that the beam can be polarized at lower energy (<70 GeV) but much more study is required to put the hope for polarized beams at high energy on firm ground. A more extended discussion of polarization in large electron storage rings can be found elsewhere[20,22].

3.1.4 Scaling of Limits with Magnetic Field of the Proton Ring

It is interesting to investigate the behaviour of the most prominent limits in the electron ring if the magnetic guiding field of the 20 TeV proton ring is different from the value (10T) chosen during this study. Any changes in the magnetic field for a fixed proton energy affects mainly the bending radius which is the same for both machines since they are housed in the same tunnel. The ratio of average radius to bending radius is assumed to be constant. The scaling laws apply to an isomagnetic electron ring.

The luminosity is hardly influenced because the number of particles per bunch N/k_b and the time between two bunch passages T_b are kept constant in order to avoid multi-bunch instabilities. The variation in geometry has some repercussion on the electron emittance and, therefore, also on luminosity. However, this relatively weak effect can easily be balanced by adjustment of N/k_b, T_b and the focussing in the e-ring.

The electric field required for acceleration scales like $E_e^4 B_p^2$, where E_e is the electron energy and B_p is the magnetic dipole field in the proton ring. The estimate shows that the electric field stays at a reasonable level over a wide range ($4 \leq B_p \leq 20$T; $40 \leq E_e \leq 200$ GeV).

It exceeds 4 MV/m only for extreme parameters occurring in the shaded area of Fig. 5.

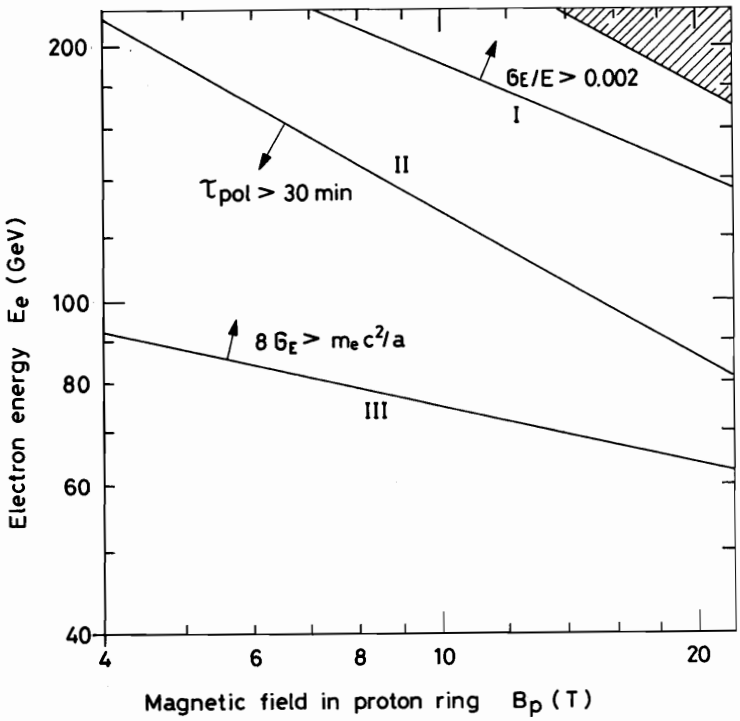

Fig. 5 Critical energies in the electron ring versus magnetic guiding field of the proton ring.

The synchrotron radiation loss per unit length follows the same scaling law. In the shaded area, it exceeds 20 kW/m which is rather high, nearly a factor 5 above the value accepted for LEP stage II (130 GeV). Since the electron current remains constant, the total synchrotron radiation power and the energy loss per turn scale with $(E_e^4 . B_p)$.

Chromaticity correction becomes difficult if the energy spread σ_E/E reaches, say, 0,002. The energy where this occurs is given by line I in Fig.5. Obviously, this effect is not very bothersome around 140 GeV.

Radiative polarization by the Sokolov-Ternov mechanism is very slow at low energies. Choosing somewhat arbitrarily 30 min as the maximum useful polarization time, line II in Fig. 5 can be drawn. At energies below this line radiative polarization must be enhanced by wigglers and, at very low energy, other mechanism as polarization by laser beams must be considered. Injection of pre-polarized beams is another possibility though very tedious operationally.

Line III indicates the electron energy where the energy spread of the beam starts to straddle integer spin resonances causing strong depolarization. At energies above this line, provisions must be made to weaken the spin resonances by precise orbit control or to suppress them altogether by complicated means such as Siberian snakes.

It is not claimed that the limits shown in Fig. 5 are fundamental; they are rather indications of the points requiring further study and effort. Although these problems are certainly not insurmountable, it is clear that the electron ring becomes more difficult if the bending radius is decreased and the electron energy kept constant. The only exception is radiative polarization which benefits from a smaller bending radius.

3.1.5 Open Problems

The following points need clarification. They are listed according to priority.

- Beam polarization and depolarization
- Beam-beam tune-shifts : Experiments are needed;
  Infl. of crossing angle, number of
  bunches and energy.
- Shielding of detector and proton beams against synchrotron radiation
- Imperfect overlap of interacting bunches : Tolerances on steering
- Provision of helicity of both signs in interaction point
- Overlap k.o. resonances : overlap of betatron and synchrotron sidebands
- Provisions for identification of proton jets[6]; usefullness[25] of mini-low-β

- Review of quadrupole lay-out in interaction region.

3.2 Electron-Proton Collisions with e-Linac and p-Ring

The electron ring could be replaced by an electron linac which provides bunches in synchronism with the proton bunches circulating in the proton ring. It is assumed that the lay-out of the interaction area is similar to that of the conventional scheme. The linac is outside the proton ring and nearly tangential to it. Only one interaction point is foreseen though the electron beam could follow a chord in the proton ring after the first interaction point and collide with the proton beam in a second interaction point.

The luminosity is given by

$$L = f_r \cdot (N_p/k_b) \cdot N_{eb} \cdot F$$

N_{eb} is the number of electrons per macro-bunch having about the same length as the proton bunch. The repetition rate f_r of the linac equals $k_b \cdot f_o$, where f_o is the revolution frequency in the proton ring. The factor F depends on beam size in the crossing point and the crossing angle. For simplicity, the beam sizes and the crossing angle are the same as in the conventional scheme (see Table 1). Since the electron beam emittance is very small the beta functions β_e^* in the electron channel can be increased to about 6 m. The luminosity aimed at is the same as in the conventional scheme.

In order to reduce the electron beam power, being proportional to $f_r \cdot N_{eb}$, the number of bunches k_b in the proton ring is reduced and the number of protons per bunch N_p/k_b is increased at the expense of the tune-shift ΔQ_e suffered by the electrons. This is admissible as the electrons are exposed only once or twice to the protons. The number of electrons per bunch N_{eb} is the same as before, in order to respect the proton tune-shift of 0,0005. Assuming that ΔQ_e can be raised to 0,06 yields the parameters given in Table 2. The disruption parameter corresponding to this tune-shift is very small $D = 1{,}9.10^{-3}$. The energy of the electron linac was chosen arbitrarily to be 100 GeV.

Table 2
Main Parameters

	p-beam		e-beam
Energy TeV	20		0,1
Luminosity $cm^{-2}sec^{-1}$		10^{31}	
Particles per bunch	3.10^{11}		$2{,}5.10^{10}$
Number of bunches	160		-
Beam-beam tune-shift	0,0005		0,06

The parameters of the superconducting, standing-wave linac are shown in Table 3. They are based on the same assumptions as used by another working group[3]. The higher mode losses are small because the peak current is relatively low. They are neglected since the efficiency of the higher-mode coupler is better than 99%. The bunch removes, per passage, 2% of the energy stored in the fundamental mode.

Table 3
Parameters of Electron Linac

Repetition frequency	kHz	660
Beam power	MW	300
Energy in one bunch	J	400
Q of S.C. cavities		10^9
Operating frequency	GHz	3
Dissipation at operating frequency at 4^oK	kW	10
Cooling power	MW	30

It is obvious from this table that the beam power is excessive implying a formidable RF generator power of more than 300 MW, much bigger than the 70 MW required by the circular electron machine which yields the same luminosity in many more interaction points. Hence, this proposition is not competitive with the conventional ep scheme and, therefore, need not be pursued further.

4. KINEMATICS, COUNTING RATES AND COMPARISON WITH FIXED TARGET μp EXPERIMENTS

4.1 Kinematics

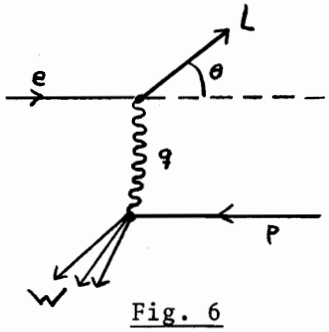

Fig. 6

In lowest order, a reaction of type ep → Lh, (L stands either for an electron or a neutrino, and h for an unspecified final hadronic state of mass W) is described by the diagram of Fig. 6, where the momentum transfer q is carried either by a photon or an intermediate boson. Denoting the four momenta of the electron, the scattered lepton and the proton by e, L

and p respectively, the kinematic variables are defined as follows :

$$s = (e + p)^2 = 4E_eE_p + M_p^2 = (\text{C.M. Energy})^2 ;$$

$$Q^2 = -q^2 = (e - L)^2 = 4E_eE_L\sin^2\frac{\theta}{2} = s \times y = \text{square of fourmomentum-transfer}$$

$$\nu = \frac{2E_p}{M_p}(E_e - E_L\cos^2\frac{\theta}{2}) = sy/2M_p ;$$

$$x = \frac{Q^2}{2M_p\nu} \quad ; \quad y = \frac{\nu}{\nu_{max}} \quad ; \quad \nu_{max} = \frac{2E_eE_p}{M_p} ;$$

with E_e = 140 GeV, E_p = 20 TeV, the present machine has $s = 1.12 \times 10^7$ GeV^2 corresponding to a C.M. energy of $\sqrt{s}$ = 3.35 TeV.

In the range of kinematics covered so far by experiments, lepton-nucleon scattering is well described in terms of the quark-parton model in which the virtual photon (or intermediate boson) emitted by the incoming lepton is absorbed by an incident quark which carries a fraction x of the momentum p of of the proton and a negligible amount of transverse momentum. After the collision the recoiling quark materializes into a jet of hadrons ("current jet") centered around the direction of the virtual photon, while the non-struck remainders of the proton give rise to a "target jet" along the incident proton direction. As shown in Fig. 7 for three different Q^2 values, the scattered lepton and the current jet are well separated in angle from each other and from the beam direction and therefore easy to detect.

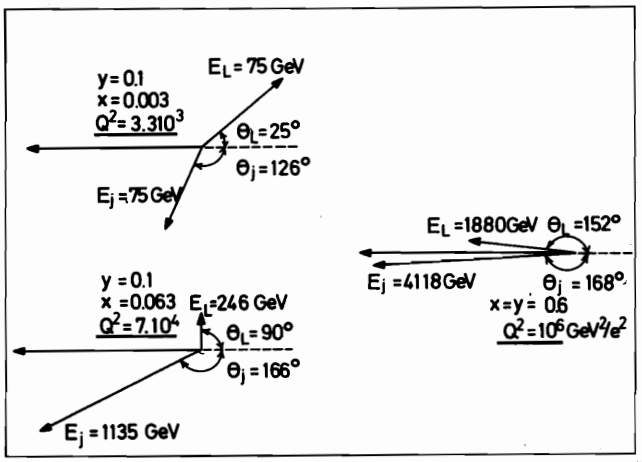

Fig. 7 Momentum vectors of the scattered electron and of the current jets for three different values of Q^2.

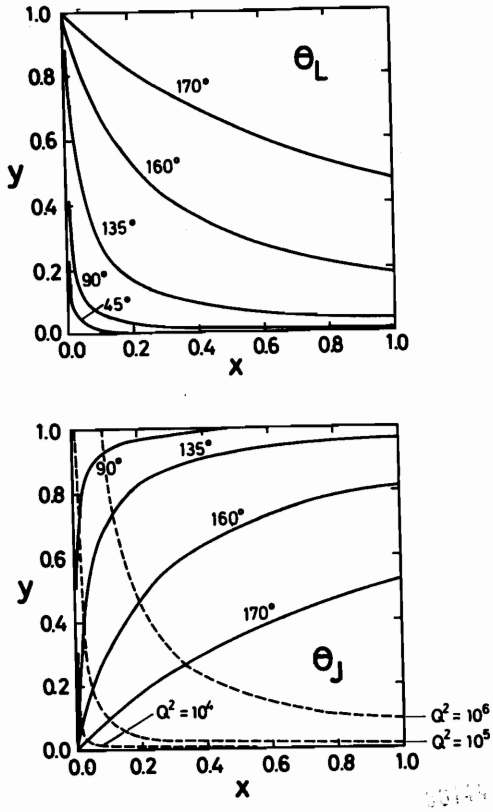

Fig. 8 Curves for fixed θ_L, θ_J and Q^2 in the x-y-plane.

This is also seen from Fig. 8, which shows curves of fixed θ_L and θ_J in the x-y-plane. The target jet, because it is centered along the beam direction will be contained in the beam pipe and therefore will escape detection by any device aiming at the observation of secondaries with substantial transverse momentum. However, as proposed by one of us[6] and discussed in chapter 5, a large fraction of the hadrons from the target jet may be observable by using the machine lattice downstream of the interaction point, interlaced with a series of calorimeters, as a hadron spectrometer.

4.2 Counting Rates and Comparison with Fixed Target μp Experiment

In trying to estimate the counting rates obtainable with the 140 GeV + 20 TeV ep collider we have to extrapolate the existing data on deep in-

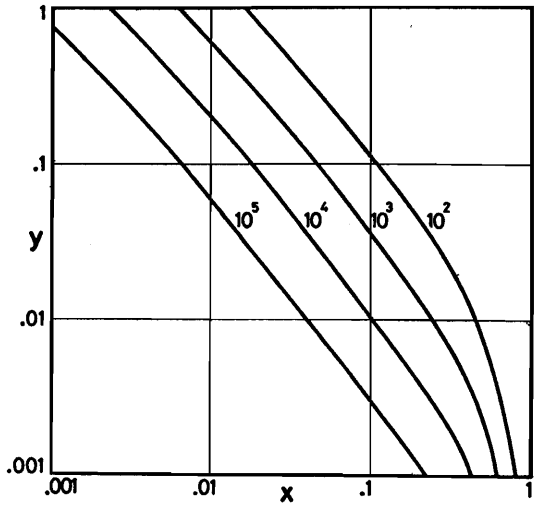

Fig. 9 Yield (ev/day/dxdy) vs. x, y (see Ref. 10)

elastic lepton nucleon scattering by more than four orders of magnitude in s and Q^2. Therefore any rates derived in this chapter must be considered very crude estimates.

Taking the structure functions of Buras and Gaemers[4] and the standard Glashow-Salam-Weinberg $SU(2)_L \times U(1)$ model with $\sin^2\theta_W = 0.23$ the cross sections for deep inelastic lepton proton scattering

$$e_L + p \to e + X \qquad (\gamma \text{ and } Z^o\text{-exchange})$$

$$e_L + p \to \nu_e + X \qquad (W\text{-exchange})$$

may be calculated.

Fig. 9 shows curves of constant differential rates in an x-y diagram for the neutral current process, as calculated by Kimura et al.[10]. The numbers in the figure represent $L \frac{d^2\sigma}{dxdy} \cdot 8{,}64 \times 10^4$ sec, the number of events per day per dxdy for a luminosity of 10^{31} $cm^{-2}sec^{-1}$. The strong variation of the differential rate with x and y exhibited by the diagram calls for fine granularity in x and y. Figs. 10, 11, 12, and 13 show the relative uncertainties in x and y due to the uncertainties in θ_L and E_L, respectively, for the detector described in chapter 5. The biggest uncertainties in x and y arise from σ_{E_L} at small values of y, corresponding to forward scattering (Fig. 8) with $Q^2 \leq 10^4$ GeV^2. With the precision assumed for θ_L and E_L in Figs. 10 - 13, Q^2 is determined with a precision of a few percent, sufficient to separate the rare large Q^2 events from the bulk of the low Q^2 events. In addition to this powerful constraint imposed by measuring angle and energy of the scattered lepton, one will use as in the case of charged current events, the angle and energy measurements of the secondary hadrons to derive x and y.

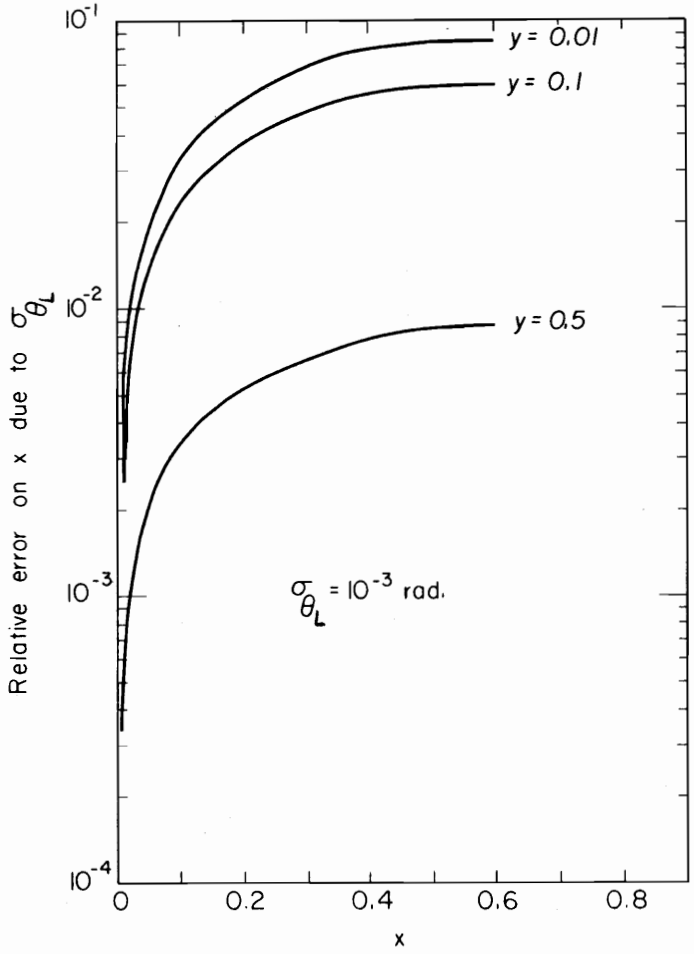

Fig. 10 Relative error on x due to σ_{θ_L} versus x.

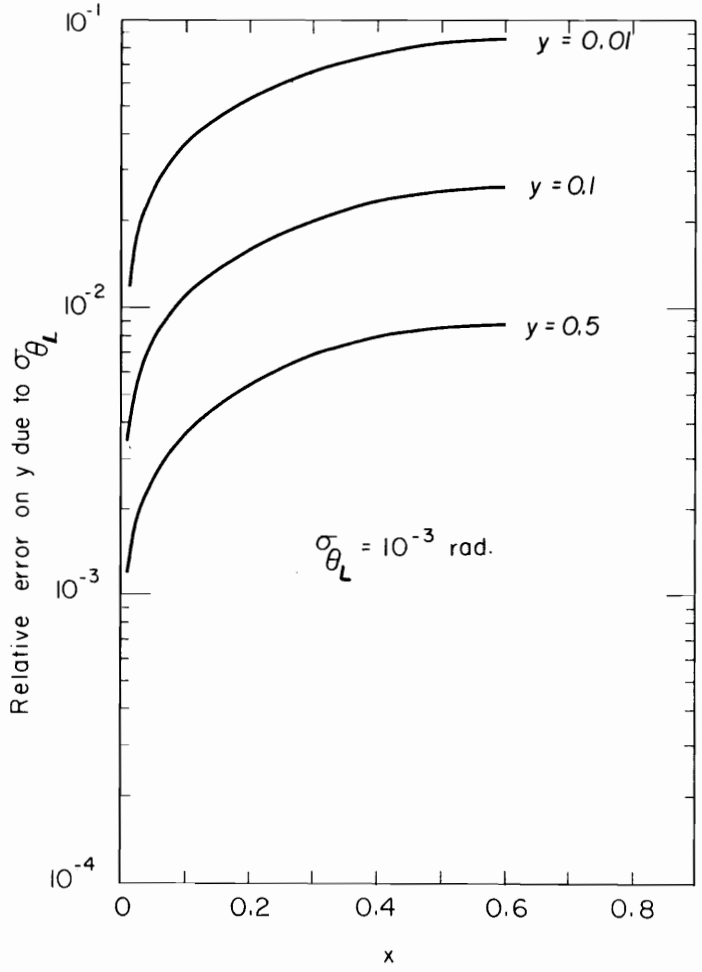

Fig. 11 Relative error on y due to σ_{θ_L} versus x.

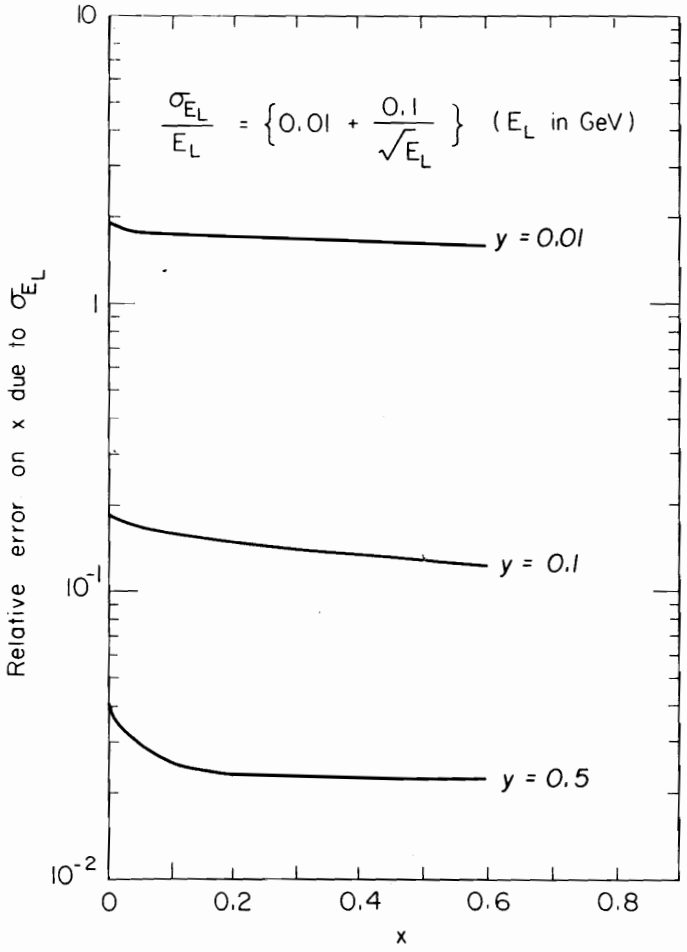

Fig. 12 Relative error on x due to σ_{E_ℓ} versus x.

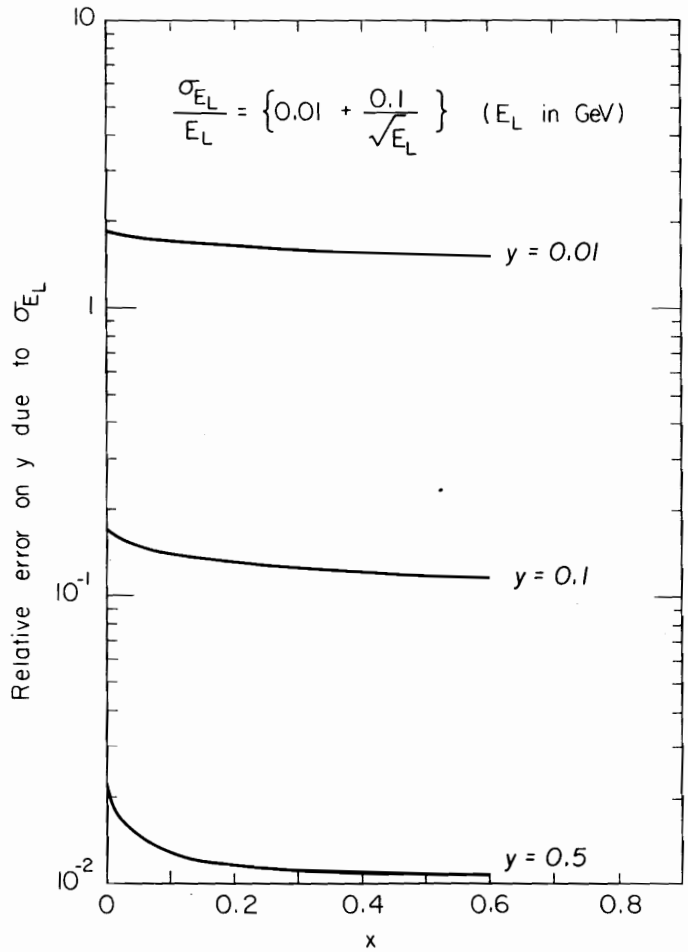

Fig. 13 Relative error in y due to σ_{E_ℓ} versus x.

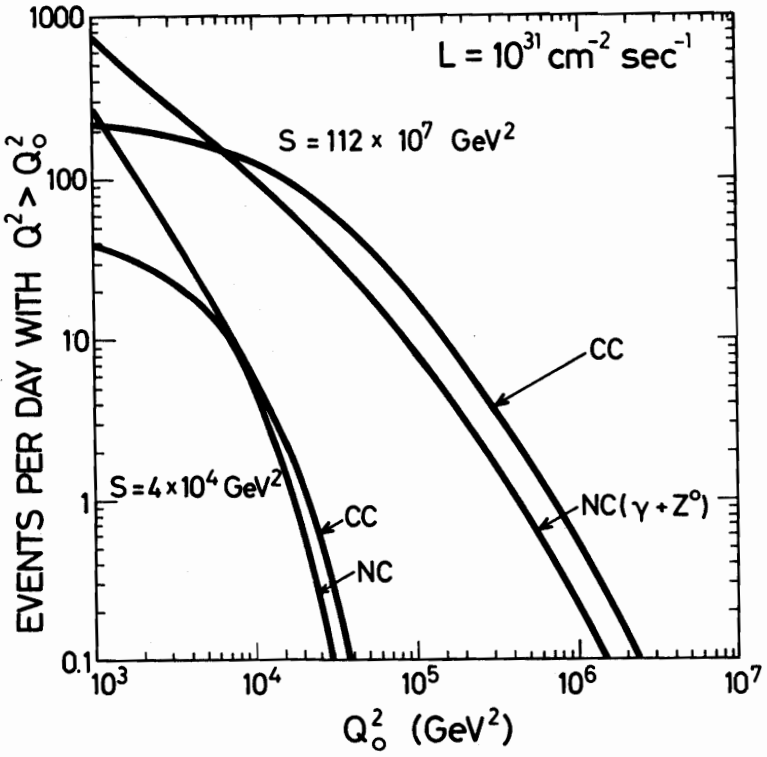

Fig. 14 Event rates per day for $Q^2 > Q_o^2$

In Fig. 14 the number of events per day with $Q^2 > Q_o^2$ is shown as a function of Q_o^2 for both the neutral and the charged current process. The rates obtained using a programme by Baroncelli and Mess[23] yield rates in good agreement with those of Kimura et al.[10]. For comparison the rates obtained for $s = 4 \times 10^4$ GeV^2 (corresponding to a 20 TeV muon beam incident on a stationary target, normalized to $L = 10^{31}$ cm^{-2}sec^{-1}) is also shown. The 20 TeV proton accelerator will have a vanishing yield of 20 TeV muons. On the other hand, as pointed out by group VI, muon fluxes of $\sim 2 \times 10^7$/sec at $E_\mu = 15$ TeV should be obtainable[5], corresponding to a luminosity of 10^{32} cm^{-2}sec^{-1} per meter of liquid H_2. Since 100 m long H_2 targets seem feasable, fixed target muon experiments will provide higher counting rates than the 140 GeV + 20 TeV ep collider at momentum transfers below $Q^2 = 10^4$GeV^2. On the other hand, the ep collider yields useful event rates up to $Q = 10^6$, a region not accessible by any fixed target device.

5. DETECTOR

As pointed out in chapter 4, it is essential for the detection of neutral current events to have a high momentum and angle resolution for the scattered electron over the full solid angle. Furthermore, good hadron calorimetry and directional analysis for the secondary hadrons are required both for charged and neutral current experiments. Because the particles

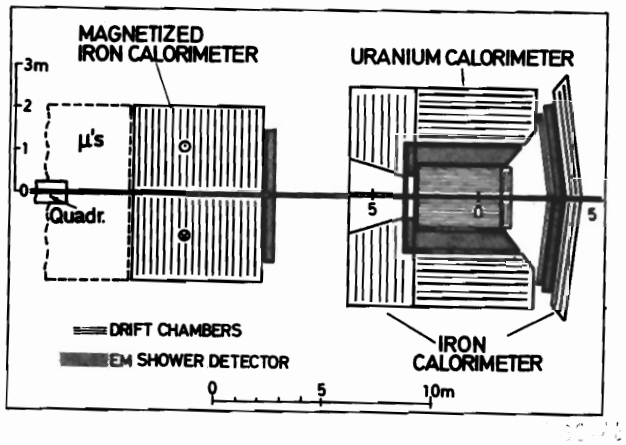

Fig. 15 Calorimetric Detector for Charged and Neutral Current Events.

belonging to the target jet will in general have their trajectories contained in the beam pipe, they will escape detection by any calorimeter centered around the interaction point. Assuming the target jet to have by vanishing transverse momentum, the scaling variables x and y, and therefore also Q^2 may be determined by measuring the total energy E_J and the angle θ_J of the current jet alone[7,9] using the following relations :

$$p_T^2 = \vec{p}_J^{\,2} \sin^2\theta_J = sxy(1 - y)$$

$$y = \frac{E_J}{2E_e} (1 - \cos\theta_J)$$

Fig. 15 shows a general purpose detector for neutral and charged current processes. It consists of a jet chamber system surrounding the interaction region backed by a system of electromagnetic and hadronic calorimeters. The angular region close to the direction of the incident protons, where the secondary particles tend to be very energetic, is covered by a magnetized iron calorimeter, preceeded by an electromagnetic shower detector and followed by a muon filter, which may incorporate the iron yokes of the first quadrupoles of the machine lattice.

Since the above expressions for p_T^2 and y are only valid to the extent that the target jet has zero transverse momentum, but the average transverse momentum associated with target fragmentation is known to be finite the detection of particles belonging to the target jet may be essential in high energy ep collider experiments.

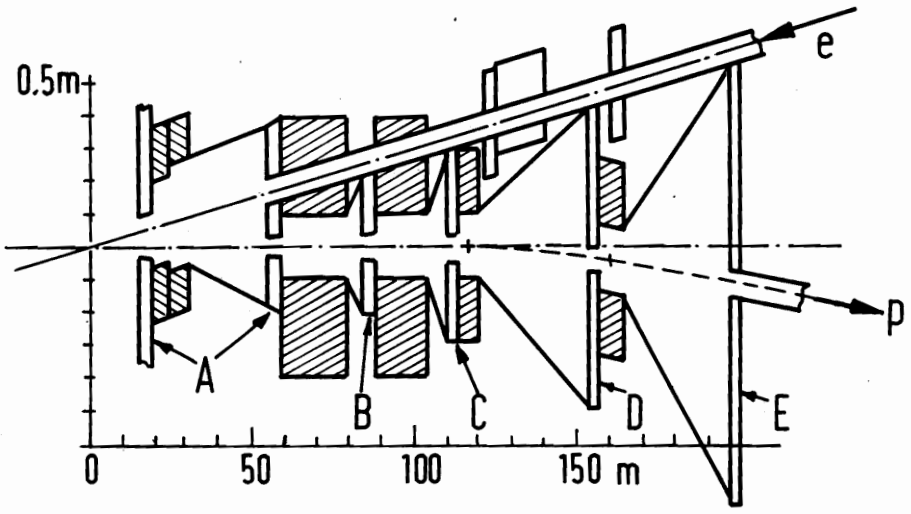

Fig. 16 Beam Pipe Spectrometer.[6] A through E are similar detection systems. For the electron insertion lenses the field gradients are ∿ 8.6T/m. Each superconducting proton lens has ∿ 100 T/m. The superconducting dipoles are of strength 66.7T-m.

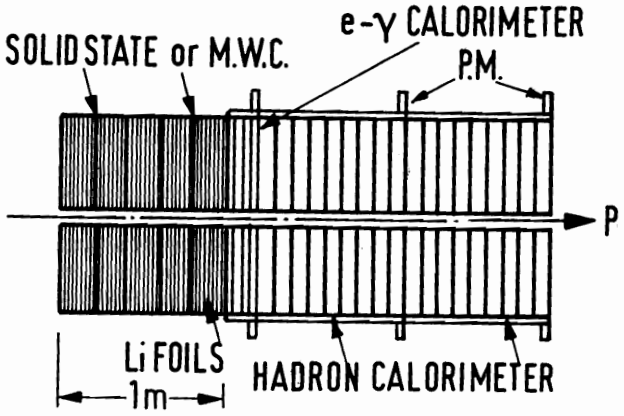

Fig. 17 One detection system.[6] The calorimeters are segmented azimuthally. The transition radiation detector gives radial and azimuthal coordinates.

Fig. 16 shows a beam pipe spectrometer[6] capable of analyzing neutral and charged secondaries with as much as 75% of the beam momentum with good efficiency. The spectrometer uses the high dispersion of the quadrupoles and dipoles of the machine lattice near the interaction region and a series of segmented transition radiation detectors followed by uranium scintillator sampling calorimeters for both e-γ and hadron energy measurement. One of these detection systems is shown in Fig. 17.

6. RADIATIVE CORRECTIONS

The interpretation of ep scattering experiments at $s \sim 10^7 GeV^2$ and $Q^2 \sim 10^4 - 10^6$ GeV^2 will require reliable calculations of the electromagnetic radiative corrections as well as the corrections due to the weak interaction. Expressing the ratio of the measured cross section $d^2\sigma$ (measured) to the lowest order cross section $d^2\sigma$ (Born) in the usual way

$$\frac{d^2\sigma \text{ (measured)}}{d^2\sigma \text{ (Born)}} = 1 + \delta(x,Q^2,s)$$

the correction term δ will have contributions from both the electromagnetic and the weak interaction. So far no specific calculations have been carried out for the ICFA collider. However, recent estimates of the electromagnetic corrections at $s = 10^5$ GeV carried out for the ep collider HERA[2] and specific calculations[24] for fixed target μp experiments at muon energies up to 30 TeV can give us an idea of the increasing importance of these corrections as the energy goes up. Fig. 18 shows an x-y plot for deep inelastic μp

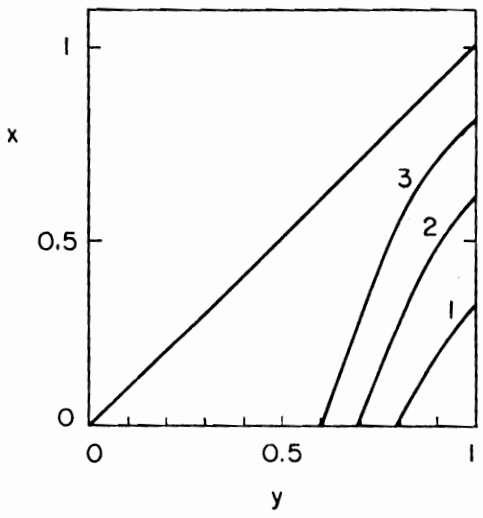

Fig. 18 Kinematical plot of the deep inelastic muon-nucleon scattering. Below the curves 1, 2, and 3, the $\delta_L^{(1)}$ is bigger than 30% at energies 300, 3000 and 30.000 GeV respectively[24].

scattering. Below the curves 1,2,3 the 1st order electromagnetic correction due to the lepton line, $\delta_L^{(1)}$ is larger than 30% at energies of 300, 3000 and 30 000 GeV respectively. The area in which the first order corrections are small is decreasing with increasing energy. This conclusion is qualitatively supported by the corrections calculated at $s = 10^5$ GeV^2 for the HERA project. Extrapolating to $s = 10^7$ GeV^2 the need for calculating the 2nd order corrections is clearly recognized.

7. CONCLUSION

The 140 GeV + 20 TeV ep collider will probe the nucleon structure down to distances inaccessible by any other means. The machine will be particularly useful for investigating left handed and right handed weak currents separately, if longitudinal electron polarization can be achieved. Using present day technology luminosities of $\sim 10^{31}$cm^{-2}sec^{-1} can be provided with interaction regions of 2 x 19 m length. Using calorimetric particle analysis based on standard technology it seems possible to study charged and neutral current phenomena at momentum transfers up to 10^6GeV^2.

REFERENCES

1) L.C. Teng (convenor); these Proceedings
2) STUDY ON THE PROTON ELECTRON STORAGE RING PROJECT HERA, ECFA 80/42, DESY HERA 80/01, March 1980.
3) E. Keil and A.N. Skrinskij (convenors), these Proceedings
4) A.J. Buras and K.J.N. Gaemers, Nucl.Phys. B134, 1249 (1978)
5) G. Barbiellini (convenor), these Proceedings. See also H.L. Anderson, LA-UR 80-520, contribution to these Proceedings.
6) W.A. Wenzel, contribution to these Proceedings
7) T. Nishikawa, Proc. IXth Int. Conf. on High Energy Accelerators, SLAC, p.584 (1974)
8) C.H. Llewellyn-Smith and B.H. Wiik, DESY 77/38 (June 1977)
9) Proceedings of the STUDY OF AN ep FACILITY FOR EUROPE, DESY 79/48 (1979);
   This report provides references to previous ECFA-studies and gives a compilation of current ep-projects.
10) Y. Kimura et al., contribution to these Proceedings
11) L.C. Teng (editor) Proc. of the Workshop on Possibilities and Limitations of Accelerators and Detectors, FNAL, Batavia (1979)
12) D. Boussard, L. Evans, J. Gareyte, T. Linnecar, W. Mills, E.J.N. Wilson, IEEE Trans. Nucl. Scie. Vol.26 (1979) 3484
    see also D. Boussard, J. Gareyte and E.N. Wilson, contribution to these Proceedings.
13) B. Zotter, private communication (1979)
14) R. Chasman and G.A. Voss, IEEE Trans.Nucl. Scie. NS-20 (1973) 777

15) K. Steffen and E. Dasskowski, contribution to these Proceedings

17) A. Hutton, Part.Acc. 7 (1976) 177

18) Ya S. Derbenev and A.M. Kontradenko, Sov.Phys. 37 (1973) 435

19) D. Möhl and B.W. Montague, Nucl.Instr.Meth. 137 (1976) 423

20) Ya. S. Derbenov, A.M. Kontradenko and A.J. Skrinskij, Part.Acc. 9 (1979) 247

21) B.W. Montague, CERN/ISR-TH/77-34 (1977)

22) J. Buon, P. Dalpiaz, Ya. Derbenev, L. Dick, G. Guignard, B.W. Montague, E. Picasso, A. Turrin, Report of the ECFA/LEP working group on beam polarization (to be published) 1979

23) The authors are indebted to Drs. Baroncelli and Mess for calculations using these programmes

24) D. Yu. Bardin et al., contribution to these Proceedings

25) K. Steffen, DESY M-79/23 (1979).